Experimental Section

Chemicals. Tetraethyl orthosilicate (TEOS), ammonia aqueous solution (NH_4OH, 28 wt.%), and dopamine hydrochloride (DA) were purchased from Aldrich. Amphiphilic block copolymer, polystyrene-*b*-poly(ethylene oxide) (PS_{173}-*b*-PEO_{170}) was purchased from Polymer Source Inc. All the chemicals were of analytical grade and were used without further purification.

Preparation of silica spheres. Silica spheres about 350 nm in size were prepared using the modified classic Stöber method. First, 9 mL of 28 wt.% $NH_3 \cdot H_2O$ was added to a mixed solution of water (16.25 mL) and ethonal (24.75 mL). An ethanolic solution of TEOS was prepared simultaneously by dissolving TEOS (2.25mL) in ethanol (22.75 mL). After stirring for 15 min, the ethanolic solution of TEOS was added to the original alkaline ethanol-water solution and the solution was reacted for another 3 hours. Silica spheres about 350 nm in size were then collected through centrifugation and washed several times with deionized water and ethanol.

Preparation of nitrogen-doped hollow mesoporous carbon spheres (NHCS-LM). In a typical synthesis of nitrogen-doped hollow mesoporous carbon spheres, 200 mg of DA was dissolved in deionized water (8 mL), and the above solution was then poured into a mixed solution of ethanol and THF (volume ratio 1:1, 8 mL) containing 30 mg of diblock copolymer (PS_{173}-*b*-PEO_{170}) and 50 mg of silica spheres about 350 nm in size under sonication. After 30 min, 0.5 mL of ammonia aqueous solution (NH_4OH, 28 wt.%) was injected to induce self-polymerization of the dopamine, and the colour of the solution turned from oyster white to dark brown. After continuous reaction for 20 hours, silica@polydopamine/diblock copolymer micelles spherical composite materials consisting silica as the core and polydopamine/diblock copolymer micelles as the shell (assigned as silica@PDA/micelles) were collected by centrifugation and washed several times with deionized water and ethanol. The wall thickness of polydopamine in silica@PDA/micelles can be adjusted by repeating the coating process. During recoating, the pre-prepared silica@PDA/micelles were used as the core instead of silica spheres, and the products were assigned as silica@PDA/micelles-2). Carbonization was performed by heating the silica@PDA/micelles under a nitrogen atmosphere at 350 ^oC for 3 hours and finally at 800 ^oC for 2 hours with a heating rate of 1 $^oC \cdot min^{-1}$. The product is assigned as silica@NMCS (NMCS refers to the nitrogen-doped mesoporous carbon shell). Finally, nitrogen-doped hollow mesoporous carbon spheres (assigned as NHCS-LM) were obtained by removing the silica template using a hydrofluoric acid aqueous solution (HF, 10 wt.%). Nitrogen-doped hollow mesoporous carbon spheres with thicker walls were also prepared by carbonization of silica@PDA/micelles-2 and removal of the silica template by HF.

Electrochemical measurements. The electrochemical measurements were conducted using traditional three-electrode system. A platinum filament and a Ag/AgCl (3 M KCl) electrode acted as counter and reference electrodes, respectively. The thin-film working electrode was prepared as follows. NHCS-LM (0.4 mg) was mixed with poly(vinylidine difluoride) (0.1 mg) and then well-dispersed in N-methylpyrrolidinone (0.2 mL) through ultrasonication. The resulting black slurry was dropped onto a graphite substrate (1 cm^2) and dried under an infrared lamp to form a thin layer. Electrochemical measurements were conducted using an electrochemical workstation (CHI 660E CH Instruments) in acid electrolytes (1.0 M H_2SO_4) at room temperature (22 °C). The electrochemical properties of the supercapacitor were studied by cyclic voltammetry (CV) and galvanostatic charge–discharge measurements. The potential sweep rate ranged from 20 to 200 $mV \cdot s^{-1}$, and the GC–DC current density varied from 1 to 10 $A \cdot g^{-1}$. The specific capacitance value was calculated from the CV curves by the following equation: $\mathbf{C} = \frac{1}{ms(V_f - V_i)} \int_{V_i}^{V_f} I(V)dv$, where m is the mass of active electrode material, s is the potential scan rate, V_f and V_i are the integration limits of the voltammetric curve, and $I(V)$ denotes the current density. The specific capacitance was calculated from the galvanostatic charge–discharge curves by the following equation, $\mathbf{C} = \frac{I \times \Delta t}{m \times \Delta V}$, C = where I is the charge–discharge current at a discharge time of Δt (s), ΔV is the potential range, and m is the mass of active electrode material.

Characterization. The morphology of the products was determined with a Hitachi SU-8000 field-emission scanning electron microscope (SEM) at an accelerating voltage of 5 kV. Transmission electron microscopy (TEM) and energy-dispersive X-ray analysis (EDXA) were conducted with a JEM-2100 at a voltage of 200 kV. The N_2 adsorption–desorption isotherms were measured using a Quantachrome Autosorb-iQ Automated Gas Sorption System at 77 K. The surface area was calculated according to the Brunauer-Emmett-Teller (BET) model using adsorption branch data in the relative pressure (P/P_0) range of 0.05-0.35. The total pore volumes and pore-size distributions were estimated from the adsorption branches of isotherms according to the nonlocal density functional theory. Wide-angle X-ray diffraction (XRD) patterns were acquired with a Rigaku Rint 2000 X-ray diffractometer using monochromated Cu Kα radiation (40 kV, 40 mA) at a scanning rate of $2° \cdot min^{-1}$. Raman spectra were collected using a Horiba-Jovin Yvon T64000 instrument with an excitation laser wavelength of λ=514.5nm. X-ray photoelectron spectroscopy (XPS) was conducted with a PHI Quantera SXM (ULVAC-PHI) instrument with an Al Kα X-ray source. All the binding energies were calibrated via referencing to the C 1 s binding energy (285.0 eV).

Figure S1

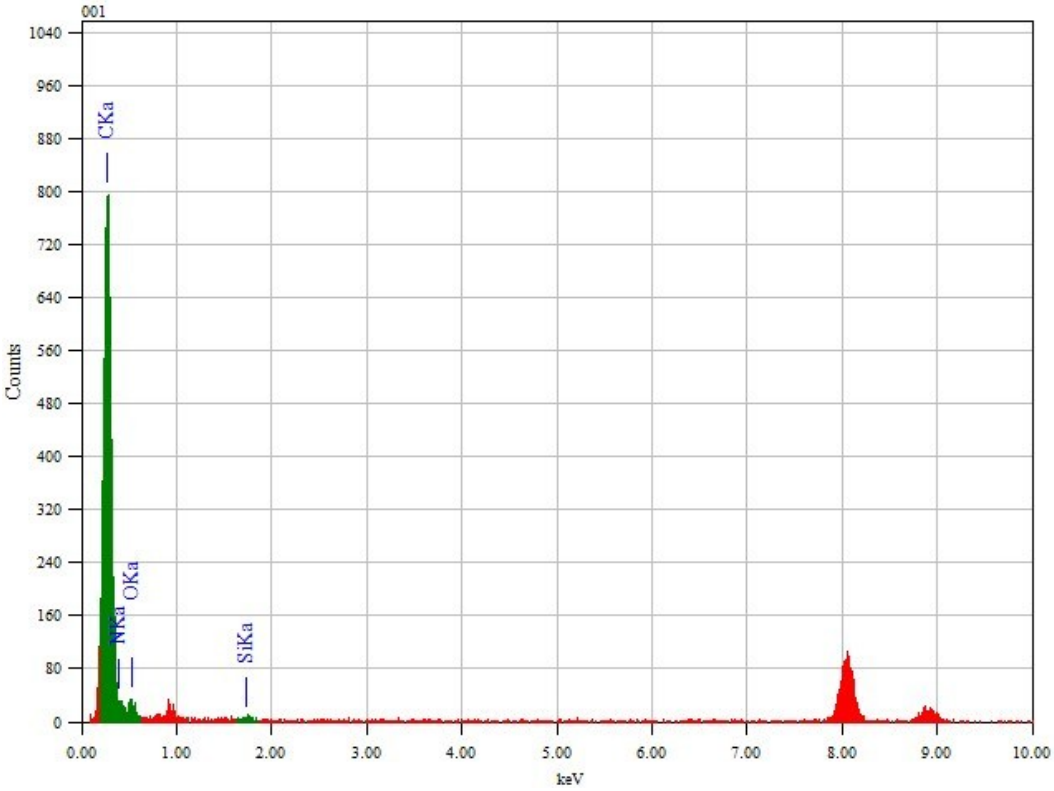

Figure S1 Energy-dispersive X-ray analysis (EDXA) of NHCS-LM.

Figure S2

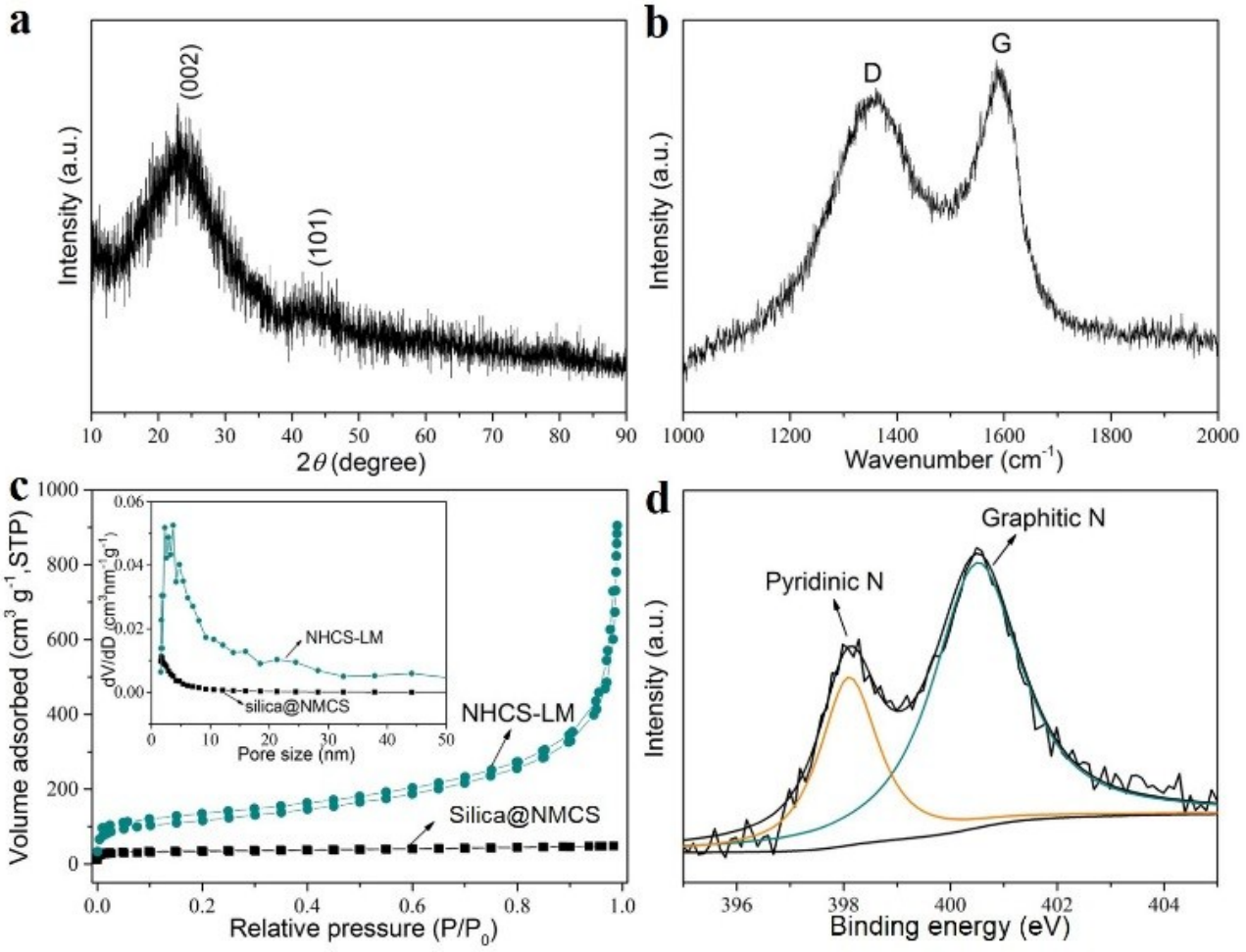

Figure S2 (a) Wide-angle XRD patterns, (b) Raman spectra, (c) nitrogen adsorption–desorption isotherms and pore-size distributions, (d) high-resolution N 1s spectrum of an NHCS-LM sample.

Note in Figure S2c-d: The porosity and electric state of nitrogen were determined by nitrogen sorption analysis (**Figure S2c**) and X-ray photoelectron spectroscopy (XPS) (**Figure S2d**). The nitrogen adsorption–desorption isotherms of the prepared silica@NMCS and NHCS-LM before and after removal of the silica template are shown in **Figure S2c**, and the inset shows the pore size distribution curves. It is clear that before removal of the silica template, the nitrogen adsorption is very low in silica@NMCS. The main nitrogen adsorption in the silica@NMCS is concentrated below a relative pressure of 0.05, due to the microporosity distribution in the shell. Silica@NMCS has a poor porosity with a BET surface area of 94 $m^2 \cdot g^{-1}$ and a total pore volume of 0.07 $cm^3 \cdot g^{-1}$. After removal of the silica core from silica@NMCS, NHCS-LM exhibit a type II isotherm which is closely associated with the macroporous texture (**Figure S2c**). Aside from the obvious existence of macropores revealed by the unsaturated nitrogen adsorption at high relative pressure ($P/P_0 > 0.9$), the nitrogen uptakes at low relative pressure ($P/P_0 < 0.05$) is caused by the presence of micropores, and the gradual nitrogen uptake in the relative pressure range of $0.05 < P/P_0 < 0.9$ is associated with nitrogen adsorption in the mesopores. The detailed micro- and meso-pore size distributions are analyzed based on nonlocal density functional theory using the adsorption branches of the isotherms, and the hierarchical pore size distributions are illustrated in the inset in **Figure S2c**. The micropores and small mesopores are mainly originated from the pyrolysis of PDA during carbonization, and the large mesopores with size around 20 nm are mostly due to the removal of the micelles as observed on SEM image (**Figure 2h**). The hierarchical porous structure of NHCS-LM leads to an increased BET surface area of 427 $m^2 \cdot g^{-1}$ and a total pore volume of 1.39 $cm^3 \cdot g^{-1}$. X-ray photoelectron spectroscopy (XPS) was also carried out, moreover, to investigate the electric state of nitrogen in the NHCS-LM. As illustrated in **Figure S2d**, the high-resolution N 1s spectrum of NHCS-LM can be fitted into two binding energies located at 398.1 and 400.5 eV, which are indexed to pyridinic-N and graphitic-N, respectively, demonstrating the successful doping of nitrogen into the carbon matrix of NHCS-LM.

Figure S3

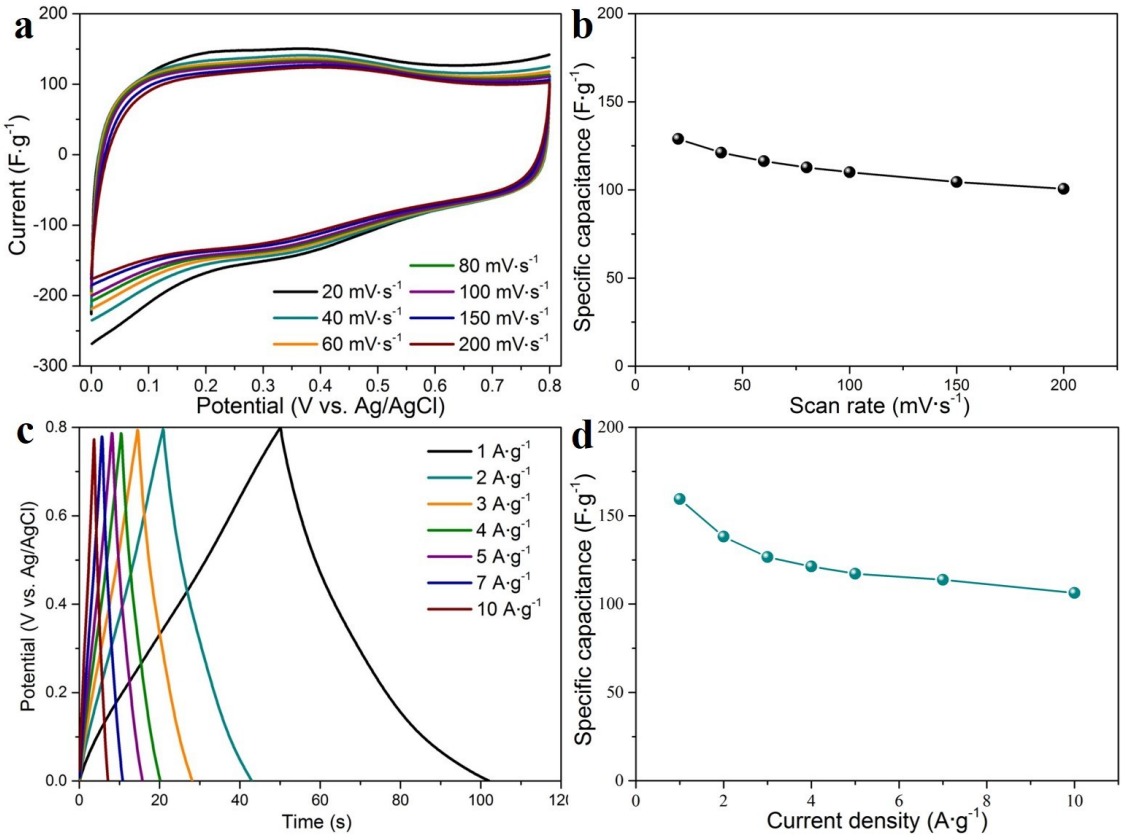

Figure S3 (a) Cyclic voltammograms with a potential sweep rate ranging from 20 to 200 $mV \cdot s^{-1}$, (b) specific capacitance values calculated from the cyclic voltammogram curves at different scan rates, (c) galvanostatic charge–discharge curves with a current density ranging from 1 to 10 $A \cdot g^{-1}$, and (d) specific capacitance values calculated from the galvanostatic charge–discharge curves at different current densities. All measurements were carried out in 1.0 M H_2SO_4 using a three-electrode system.

Note in Figure S3: The electrochemical properties of a NHCS-LM electrode implemented in a supercapacitor architecture were investigated by cyclic voltammetry (CV) and galvanostatic charge-discharge (GC-DC) measurements (**Figure S3**). The system was constructed in a three-electrode system with a 1 M H_2SO_4 aqueous electrolyte. The CV curves were recorded at sweep rates ranging from 20 to 200 $mV \cdot s^{-1}$. Galvanostatic charge-discharge measurements were obtained at various current densities ranging from 1 to 10 $A \cdot g^{-1}$. It was observed that the NHCS-LM presented quasi-rectangular CV curves with a distinct hump (**Figure S3a**) and displayed quasi-linear charge-discharge curves accompanied by a slight bend (**Figure S3c**). These phenomena indicate that the capacitive response of NHCS-LM combines electric double-layer capacitance originating from the porous carbon with pseudo-capacitance originating from the doped nitrogen atoms.[R1,R2] It is noteworthy that the quasi-rectangular CV curves are only slightly distorted (**Figure S3a**), even at a high potential sweep rate of 200 $mV \cdot s^{-1}$, implying an efficient ion transfer and rapid ion response inside the NHCS-LM electrode. The diffusion pathways and transport resistance of the electrolytes and ions are minimized due to the unique structural properties of NMCS-LM. This is because the macroporous core of in NMCS-LM is able to build a buffer space for the electrolytes and the mesoporous thin wall provides free pathways for the ions, conditions favoring high-rate operation.[R3,R4] The specific capacitance values calculated from both the CV and galvanostatic charge-discharge curves are plotted in **Figures S3b,d**. The NHCS-LM electrode shows a specific capacitance of 130 $F \cdot g^{-1}$ and 160 $F \cdot g^{-1}$ at a scan rate of 20 $mV \cdot s^{-1}$ and a current density of 1 $A \cdot g^{-1}$, respectively.

[R1] F. W. Ma, H. Zhao, L. P. Sun, Q. Li, L. H. Huo, T. Xia, S. Gao, G. S. Pang, Z. Shi, S. H. Feng, *J. Mater. Chem.* **2012**, *22*, 13464–13468.

[R2] L. F. Chen, X. D. Zhang, H. W. Liang, M. G. Kong, Q. F. Guan, P. Chen, Z. Y. Wu, S. H. Yu, *ACS Nano* **2012**, *6*, 7092–7102.

[R3] D. W. Wang, F. Li, M. Liu, G. Q. Lu, H. M. Cheng, *Angew. Chem. Int. Ed.* **2008**, *47*, 373–376.

[R4] K. S. Xia, Q. M. Gao, J. H. Jiang, J. Hu, *Carbon* **2008**, *46*, 1718–1726.